JOURNAL OF GEOPHYSICAL RESEARCH, VOL. 106, NO. C5, PAGES 9509–9516, MAY 15, 2001

Spectral particulate attenuation and particle size distribution in the bottom boundary layer of a continental shelf

Emmanuel Boss,[1] W. Scott Pegau,[1] Wilford D. Gardner,[2] J. Ronald V. Zaneveld,[1] Andrew H. Barnard,[1] Michael S. Twardowski,[1] G. C. Chang,[3,4] and T. D. Dickey[3]

Abstract. Spectral attenuation and absorption coefficients of particulate matter and colocated hydrographic measurements were obtained in the Mid-Atlantic Bight during the fall of 1996 and the spring of 1997 as part of the Coastal Mixing and Optics experiment. Within the bottom boundary layer (BBL) the magnitude of the beam attenuation decreased and its spectral shape became steeper with distance from the bottom. Concurrently, the slope of the particulate size distribution (PSD) was found to increase with distance from the bottom. Changes in the PSD shape and the magnitude of the beam attenuation as functions of distance from the bottom in the BBL are consistent with particle resuspension and settling in the BBL, two processes that are dependent on particle size and density. For particles of similar density, resuspension and settling would result in a flattening of the PSD and an increase in the beam attenuation toward the bottom. In both fall and spring the magnitude of the particle attenuation coefficient correlates with its spectral shape, with a flatter shape associated with higher values of the attenuation. This observation is consistent with idealized optical theory for polydispersed nonabsorbing spheres. According to this theory, changes in the steepness of the particle size distribution (particle concentration as a function of size) will be associated with changes in the steepness of the attenuation spectra as a function of wavelength; a flatter particle size distribution will be associated with a flatter attenuation spectrum. In addition, the observed ranges of the beam attenuation spectral slope and the PSD exponent are found to be consistent with this theory.

1. Introduction

The beam attenuation coefficient is an important optical property of ocean water used both to quantify light propagation in the ocean and to study the concentration of the material affecting light propagation. The beam attenuation is decomposed to the attenuation by particles, dissolved material, and the water itself. Of these components, particulate attenuation is the most variable in the ocean. With the advent of a high-frequency spectral attenuation meter [*Moore et al*., 1996], high vertical resolution spectral measurements of beam attenuation have become routine. While the magnitude of the beam attenuation has been used extensively to study the distribution of particulate matter in the ocean [e.g., *Gardner et al*., 1993; *McCave*, 1983; *Pak et al*., 1980], retrieving additional information from its spectral shape has received little attention (exceptions are *Volz* [1954], *Morel* [1973], *Kitchen et al*. [1982], and *Barth et al*. [1997]). The main objective of this paper is to study the relationship between the spectrum of particulate attenuation and the shape of the particulate size distribution. We use field observations to test a theoretical model [*Volz*, 1954; *Morel*, 1973; *Diehl and Haardt*, 1980] linking the spectral shape of the particle attenuation and the particle size distribution. Knowledge of the particulate size distribution (PSD) shape is of great use for computing sinking rates of suspended particles. It is also an important parameter in models that compute the bulk particulate index of refraction (and thus composition) from the particulate backscattering to particulate scattering ratio (M. S. Twardowski et al., Model for retrieving oceanic particle composition and particle distribution from measurements of the backscattering ratio and spectral attenuation, submitted to *Journal of Geophysical Research*, 2000, hereinafter referred to as Twardowski et al., submitted manuscript, 2000).

PSDs in the ocean are often found to be well approximated by a hyperbolic (Junge-like) distribution,

$$N(D) = N_0(D/D_0)^{-\xi}, \tag{1}$$

where $N(D)$ is the number of particles per unit volume per unit bin width (see notations). The exponent of the PSD, ξ, typically varies between 3 and 5 [e.g., *Diehl and Haardt*, 1980; *McCave*, 1983; *Morel*, 1973]; that is, there are numerically many more small particles than big ones. Under the anomalous diffraction model of *van de Hulst* [1957], which assumes that the particle's index of refraction is close to that of water, for nonabsorbing particles with a spectrally constant (real) index of refraction and with a Junge-like PSD, the particulate attenuation c_p depends on the wavelength according to [*Diehl and Haardt*, 1980]

$$c_p(\lambda) = A\lambda^{-\gamma}. \tag{2}$$

For this solution the exponent of the particulate attenuation spectrum (the hyperbolic exponent, γ) as a function of wave-

[1]College of Ocean and Atmospheric Science, Oregon State University, Corvallis.
[2]Department of Oceanography, Texas A&M University, College Station.
[3]Ocean Physics Laboratory, University of California, Santa Barbara, Goleta.
[4]Now at Florida Environmental Research Institute, Tampa.

Paper number 2000JC900077.
0148-0227/01/2000JC900077$09.00

length and the exponent of the PSD (ξ) are linearly related by [*Diehl and Haardt*, 1980]

$$\gamma = \xi - 3. \quad (3)$$

Therefore, under the above assumptions the shape of the attenuation spectrum is fully specified by the PSD. Note, however, that the anomalous diffraction approximation is not applicable for the smallest particles [*Shifrin*, 1988; *van de Hulst*, 1957] contrary to the assumption used in deriving (3) [*Diehl and Haardt*, 1980]. We are currently investigating theoretically the range of applicability of (3) for more general types of oceanic particles (E. Boss and M. S. Twardowski, The shape of the particulate beam attenuation spectrum and its relationship to the size distribution of oceanic particles, submitted to *Applied Optics*, 2000, hereinafter referred to as Boss and Twardowski, submitted manuscript, 2000).

Here we investigate whether the shape of the attenuation spectrum $c_p(\lambda)$ of absorbing, polydispersed oceanic particles is well approximated by a wavelength dependence of the form $\lambda^{-\gamma}$ (2) and whether γ varies in relation to changes in the beam attenuation magnitude and ξ (3). Since phytoplankton have an index of refraction that is highly variable as a function of wavelength [*Stramski and Mobley*, 1997], we attempt the comparison in the region of the water column where particles are expected to be more uniform in their index of refraction, the bottom boundary layer (BBL). In the BBL over the continental shelf the particles are dominantly detritus and weakly absorbing sediments. If we cannot find a relationship between the attenuation spectrum and the size distribution for these particles, then we are likely to fail in the much more complex phytoplankton-dominated water column higher up.

In the BBL the particle size distribution is dependent, to first order, on resuspension and settling. Both resuspension and settling are dependent on the particle's size and density. The settling velocity of particles denser than the surrounding water increases monotonically with particle size. For particles in the range of interest the Reynolds number is small, and Stokes' law generally applies, with the settling velocity scaling with the diameter squared. Similarly, resuspension is particle size–dependent, with higher bottom shear stress needed to suspend bigger (and/or denser) particles [*Miller et al*., 1977]. This implies that the PSD will change as a function of depth near the seafloor; closer to the bottom, relatively more big particles are expected to be present in comparison to higher up in the BBL. In terms of a fitted Junge-like distribution we expect the PSD exponent ξ to increase with distance from the sediment bed. This trend is predicted by the simplest steady state model for particle resuspension, in which turbulent diffusion equals settling [*Rouse*, 1937]. While this model has several limitations, experimental and observational evidence support it [*Middleton and Southard*, 1984].

Particulate attenuation c_p is expected to decrease with increasing distance from the bottom as the concentration of particles decreases. In short, in the BBL the magnitudes of both the c_p and ξ are expected to change monotonically as functions of distance from the bottom. For a polydispersion of particles, all having a similar index of refraction, we expect the hyperbolic fit exponent γ to decrease with the flattening of the PSD near the bottom (3). According to the previous arguments the shape of c_p (described by γ) should covary with the shape of the PSD (ξ); thus we expect the magnitude of c_p and its shape γ to be correlated for resuspended particles. Because for simplified Mie theory γ increases with increasing ξ, we expect γ to decrease with increasing c_p.

Experimental evidence shows that γ and ξ are related in the ocean; *Kitchen et al*. [1982] found a significant correlation between the ratio of $c_p(450)/c_p(650)$ and ξ measured by Coulter counter, thus establishing the link for oceanic particles between the shape of the attenuation and the shape of the size distribution. To obtain the particulate attenuation, *Kitchen et al*. [1982] estimated the attenuation due to water and colored dissolved organic matter (CDOM) on the basis of attenuation of the clearest water (i.e., assuming that it is constant throughout the water column). Here we refine this study by directly measuring the absorption by the dissolved fraction to obtain the particulate attenuation by subtraction from the total attenuation coefficient (we assume the attenuation and absorption in the dissolved fraction to be equal).

2. Methods

Hydrographic and optical data were collected during two cruises in the Mid-Atlantic Bight: Coastal Mixing and Optics experiment I (CMO I), August 17 to September 7, 1996, and CMO II April 26 to May 13, 1997). The data presented here are from a time series station located at ~70 m depth (40.5°N, 70.5°W) *Gardner et al.* [this issue] and *Chang and Dickey* [this issue] for a general description of hydrographic, optical, and particulate property distributions throughout the experiment). The area where the data were collected is known as the Mud Patch, a 2–14 m thick deposit of fine-grained material overlying coarser sand-sized sediment covering an area of 100 by 200 km [*Twichell et al*., 1987]. Intense storms (wind stress >0.4 N m^{-2}) occurred during both cruises, causing a wide range of particulate concentrations near the bottom [*Dickey et al*., 1998]; during CMO I (September 2, 1996) the eye of Hurricane Edouard passed 110 km from the time series station while a series of spring storms passed over the site during CMO II.

Two WET Labs ac-9s were used to measure CDOM absorption a_g and absorption and attenuation of dissolved plus particulate coefficients (a_{pg} and c_{pg}). To determine the contribution of dissolved materials to a_{pg} and c_{pg}, a 0.2 μm filter (Gelman Suporcap 100) was attached to the inlet of one ac-9. Both instruments were calibrated daily with optically pure water as a reference (Barnstead NANOpure). The particulate absorptions a_ps were corrected for scattering following method 3 (CMO I) and method 1 (CMO II)of *Zaneveld et al*. [1994]; a_p and c_p were calculated by subtracting the absorption of the fraction smaller than 0.2 μm (a_g) from a_{pg} and c_{pg}.

Hydrographic properties were measured on the same package (the Slow Descent Rate Optical Profiler) (SlowDROP) with a SeaBird Electronics SBE-911 conductivity-temperature-depth profiler (CTD) (a SBE-25 CTD was used after April 30). The data from the CTD and ac-9 were merged and binned to 1 m intervals. Data were collected in sampling bursts (an average of 3 d^{-1}) that lasted an average of 40 min (+/−10 min) with an average of four casts per burst. All points with a density within 0.01 kg m^{-3} of the density of the deepest measurement in a given cast were assumed to be in the BBL. The BBL was typically 10 m deep in the fall and 20 m deep in the spring [*Gardner et al.*, this issue].

A bio-optical system containing an ac-9 was also moored 2 m above the bottom on a tripod from August 9 to September 26, 1996 (deployment I), from September 27, 1996, to January 2, 1997 (deployment II), and from April 17 to June 11, 1997

(deployment IV), at the CMO site (see *Chang and Dickey* [this issue] and *Chang et al*., [this issue] for more details regarding the tripod). From the tripod data set we use 8 hour averaged ac-9 spectral beam c data to compare with out measurements higher in the water column and to assess the variability throughout the year. All the other measurements presented here were conducted from research vessels that were located between 1 and 5 miles away from the tripod.

PSDs were measured using a Coulter Multisizer with a 50 μm aperture size and a 0.5 mL sample volume. PSDs could therefore be resolved between 1 and 30 μm. We use only the 2–20 μm range to eliminate possible noise in the small size range and because the scarcity of particles >20 μm made statistics poor (*Blakey et al*., submitted manuscript, 2000). Samples for particle analysis were taken using the ship's rosette package at different times than the profiles of the SlowDROP (time difference 1–3 hours). We used data from a beam transmissometer (SeaTech, 660 nm) on the CTD package to relate the PSD to the magnitude of the attenuation coefficient. Since the attenuation by CDOM is very small at that wavelength and the attenuation by water is nearly constant and subtracted from c_{pg}, we refer to the remaining value for the beam transmissometer on the rosette as particulate attenuation ($c_p(660)$). Note that we do not have colocated spectral particulate attenuation measurements and PSD measurements. The two were connected through their correlation with $c_p(660)$.

The attenuation spectra from the ac-9 were least squares fit to the function $c_p(\lambda) = \tilde{c}_p(660)(\lambda/660)^{-\gamma}$ using the 412, 440, 488, 510, 532, 555, 650, and 676 wave bands of the ac-9. Here $\tilde{c}_p(660)$ denotes the magnitude of the fitted attenuation spectra at 660 nm. The average rms difference between measured and fitted amplitudes at all measured wavelengths was 0.0015 m^{-1}, significantly smaller than the instrument precision [*Twardowski et al.*, 1999]. The reference wavelength chosen (660 nm) does not influence the exponent of the fit (γ) and was chosen for comparison with the single wavelength beam transmissometer on the CTD rosette. A similar fit with the same wavelengths was applied to c_{pg} for comparison with the tripod data. In that case the model is $c_{pg}(\lambda) = \tilde{c}_{pg}(660)(\lambda/660)^{-\gamma_{pg}}$. The γ_{pg} values were greater than γ because of the contribution of the CDOM shape to the shape of the c_{pg} (CDOM absorption spectra in the visible are well approximated by a decreasing exponential as a function of wavelength).

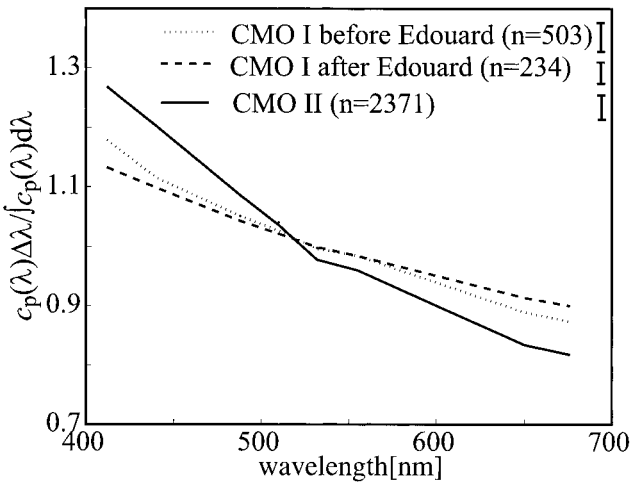

Figure 1. Medians of the area-normalized shape of the particle attenuation spectra $c_p(\lambda)$ (the average of normalized shape is 1). Bars on the right-hand side denote the mean deviation from the 16th to the 86th percentile. Numbers in parentheses denote the number of spectra used for the analysis.

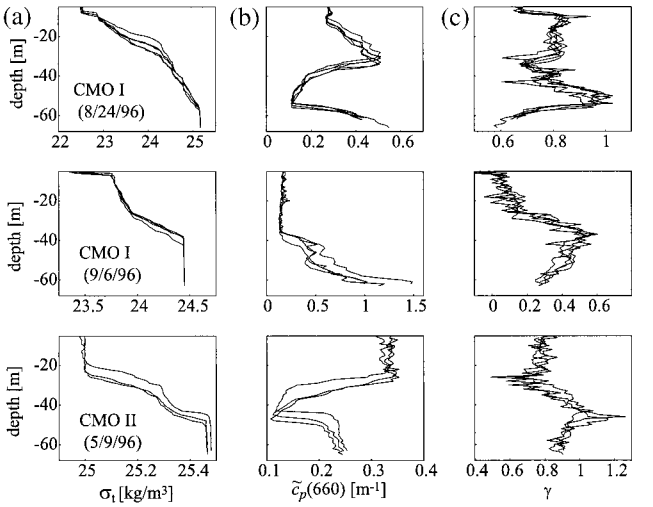

Figure 2. (a) Representative depth profiles of density σ_t, (b) the magnitude ($\tilde{c}_p(660)$), and (c) the exponent of a hyperbolic fit (γ) to the particulate attenuation. Data from consecutive profiles (typically within 40 min) in the fall during CMO I prior to Hurricane Edouard (August 24, 1996), during CMO I following the hurricane (September 6, 1996), and in the spring during CMO II (May 9, 1997). BBL is typically only the bottom 10–20 m of each profile. Note the different scales.

The errors associated with the measurements are property- and wavelength-dependent. Here c_{pg} and a_g were directly measured and have a maximum error of ± 0.005 m^{-1} based on the ac-9 measurement precision. The error in c_p values is smaller than the ± 0.007 m^{-1} based on the propagation of the instrumental error. An additional error may arise for imperfect colocation of the filtered ac-9 and unfiltered ac-9 measurements because of filter-induced delays. Observed vertical gradients in CDOM were no bigger than 0.0005 m^{-1} per vertical meter at 440 nm [*Boss et al*., this issue]. This error is not expected to cause a noticeable change in the magnitude of c_p. This error may, however, induce a bias in the shape. The binning of data to 1 m intervals is expected to reduce further errors in c_p and its spectral fit.

3. Results

3.1. Optical Data

Particulate attenuation spectra from the BBL were fit well with the hyperbolic model of (2). The average shape of all three sampling periods, before and after the hurricane in CMO I and CMO II, had statistically significant curvatures (positive second derivatives with wavelength, Figure 1). The averaged (over all the data in the BBL) rms difference between the nonlinear fit and the attenuation spectrum was half that of the linear fit (0.0015 versus 0.003 m^{-1} at each wavelength), implying its superiority. The change in the average spectral shape of c_p between CMO I and CMO II was larger than the difference before and after the hurricane (Figure 1). The variance in shape was biggest before the hurricane (Figure 2). In average,

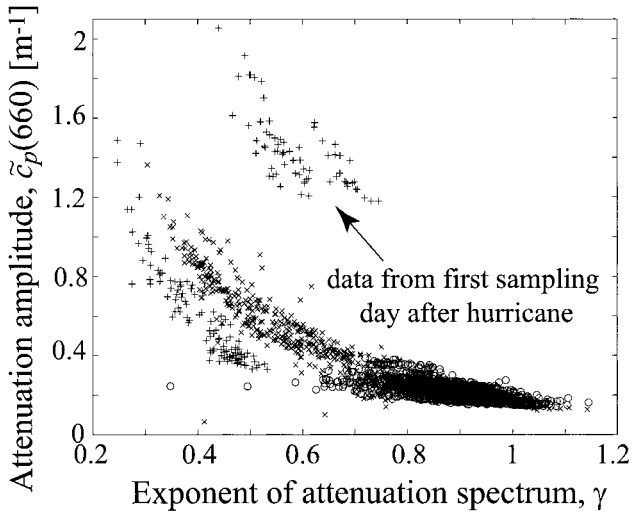

Figure 3. Parameters of the least squares fit model of the attenuation spectra $c_p(\lambda) = \tilde{c}_p(\lambda/660)^{-\gamma}$ for all the data from the BBL at the time series station for CMO I data before the hurricane (crosses), CMO I data after the hurricane (pluses), and CMO II data (open circles). The data are the same as those used in Figure 1.

smaller values of attenuation were observed in CMO II (Figures 2 and 3).

Typical distributions of density, $\tilde{c}_p(660)$ and γ, for sampling bursts in each sampling period (Figure 2) illustrate that (1) γ varied smoothly as a function of depth, (2) within the BBL (bottom 10–20 m), $\tilde{c}_p(660)$ increased while γ decreased with depth, and (3) within the duration of the sampling bursts (O(40 min)), variability was observed in both $\tilde{c}_p(660)$ and γ. Here γ correlated negatively with $\tilde{c}_p(660)$ in both CMO I and CMO II. The distributions of $\tilde{c}_p(660)$ and γ were relatively tight except for the sampling period following Hurricane Edouard (Figure 3). The correlation coefficient between γ and $\tilde{c}_p(660)$ was 0.87 for the data excluding the period following the hurricane. Figure 3 suggests a nonlinear relationship such as

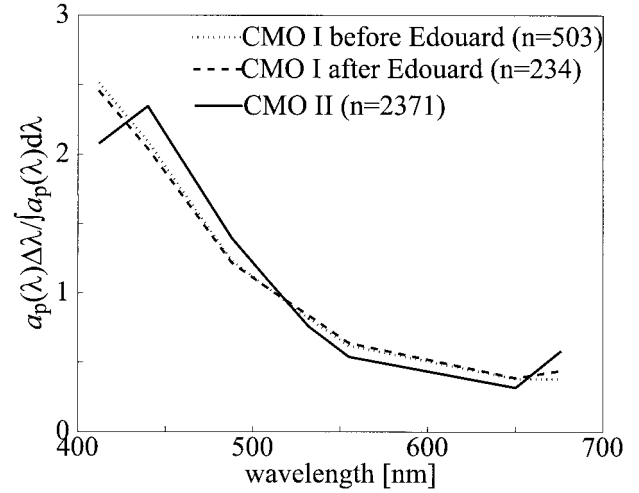

Figure 4. Medians of the area-normalized shape of particulate absorption $a_p(\lambda)$ (the average of normalized shape is 1). The deviations from the 16th to the 86th percentile were smaller than 0.05 m^{-1} and are not displayed. Numbers in parentheses denote the number of spectra used for the analysis.

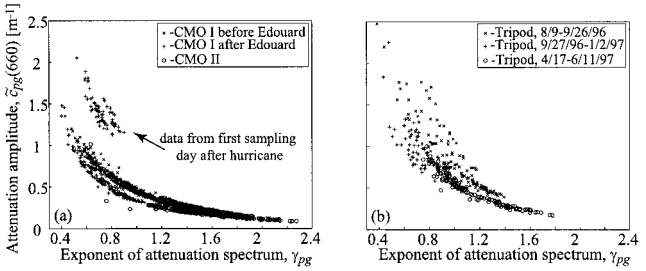

Figure 5. Parameters of the least squares fit model to the beam attenuation spectra $c_{pg}(\lambda) = \tilde{c}_{pg}(660)(\lambda/660)^{-\gamma_{pg}}$ for all the data from the BBL at the time series station (a) for both CMO cruises and (b) from the tripod data at 2 m above bottom.

$\tilde{c}_p(660) \propto 1/\gamma$; regressing $\tilde{c}_p(660) \propto 1/\gamma$ using the same data results in a correlation coefficient of 0.93.

The initial data taken after the hurricane passage had a different $\tilde{c}_p(660) - 1/\gamma$ relationship than observed in the data from before the hurricane. Two days later this relationship was more similar to the observation made prior to Hurricane Edouard (Figure 3).

The type of particles observed in the BBL can be inferred from the particulate absorption spectra and the ratio of particulate scattering and attenuation. The mean of the area-normalized absorption spectra typically corresponded to detritus (i.e., proportional to $\exp(-0.01\lambda)$, Figure 4). A noticeable Chl *a* peak was observed during CMO II; yet, even then, the absorption spectrum is dominated by detritus, as is evident from the absorption ratio of 440–676 nm. Typical absorption blue/red ratios for phytoplankton vary from 1.5 to 2.8 [*Culver and Perry*, 1999], while for detritus the ratio is nearly 10. The single scattering albedo for particles, the ratio of scattering to attenuation, b_p/c_p, during CMO I (CMO II) varies from 0.86 ± 0.02 (0.82 ± 0.04) for $\lambda = 412$ nm to 0.97 ± 0.01 (0.92 ± 0.03) for $\lambda = 676$ nm, indicating the dominance of scattering relative to absorption at all wavelengths. This suggests that the BBL was dominated by detritus and resuspended sediments.

The same functional fit ($\propto \lambda^{-\gamma}$) was also found to be applicable to c_{pg}. Here $c_{pg}(\lambda)$s were more concave than $c_p(\lambda)$s because of the decreasing exponential shape of $a_g(\lambda)$. Values of γ_{pg} were significantly larger than γ (compare Figures 3 and 5); while $\tilde{c}_{pg}(660)$ was bigger than $\tilde{c}_p(660)$ by <5%, the exponent of the hyperbolic fit (γ_{pg}) increased by as much as

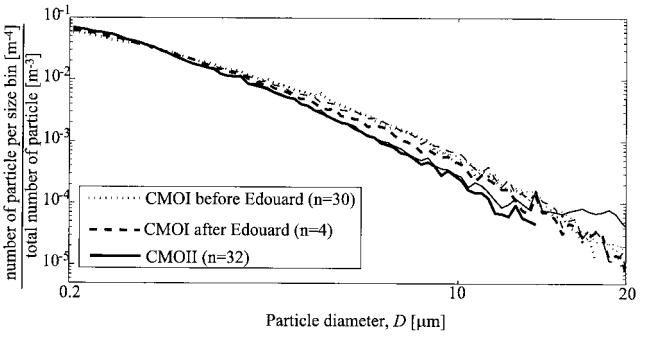

Figure 6. Mean (thin line) and median (thick line) of the area-normalized particle size distribution shape of all data of each sampling period. When no values are present, zero particles median or mean were recorded.

Table 1. Observed Ranges of the PSD Exponent ξ for Two Different Particle Size Ranges and the Exponent of the Hyperbolic Fit to the Spectral Attenuation γ

	$c_p(660)$	Range of ξ for $2 < D < 20\ \mu$	Range of ξ for $3 < D < 20\ \mu$	Range of γ
CMO I	0.3–1.5	2.5–3.2	3–3.5	0.3–1.1
CMO I, (first 25 hours of sampling after the hurricane passage)	1.3–2	2.5–3.1	3.5–3.7	0.45–0.7
CMO II	0.15–0.35	3.1–3.9	3.3–4.1	0.7–1.15

Both are given for a range of $c_p(660)$ observed on both the SlowDROP (where spectral c_p was measured) and on the CTD package (with which the water sample was collected and a single wavelength beam-c measured).

180% relative to γ, with the largest changes occurring at small attenuation magnitudes, where the dissolved attenuation is a higher fraction of c_{pg}. The tripod data exhibited a higher variability; yet still, a significant $\bar{c}_{pg}(660) - \gamma_{pg}$ relationship was observed (Figure 5b, linear correlation coefficient of 0.44). Except for the first deployment and for high attenuation values ($\bar{c}_{pg}(660) > 1.3\ \mathrm{m}^{-1}$) the $\bar{c}_{pg}(660) - \gamma_{pg}$ relationship is similar to that observed with the SlowDROP.

3.2. Particle Data

PSDs within the BBL were generally steeper during CMO II than during CMO I (Figure 6). The shape of the PSD is most variable for the period after the hurricane (highest standard deviation, not shown). A single Junge exponent was found not to match very well the whole data from 2 to 20 μ; A better fit, yet with a significantly higher exponent, was found when the size range was limited to $3 < D < 20\ \mu$ (Figure 6 and Table 1).

Significant differences were found in the PSD exponent ξ between the different sampling periods; for values of $c_p(660) < 1\ \mathrm{m}^{-1}$ the trend was for ξ to decrease monotonically with attenuation, though the scatter was large. The large values of $c_p(660)$ occurred just before and after the passage of Hurricane Edouard. Consistent with the change in ξ, for values of $c_p(660) < 1\ \mathrm{m}^{-1}$ the mean particle size increased with attenuation (not shown).

In order to estimate how much of the particulate attenuation could be explained by the observed PSD we computed the average particle attenuation efficiency factor (the ratio of attenuation to the total surface area of the particles, $\langle Q_c \rangle$):

$$\langle Q_c(660) \rangle \equiv c_p(660) / \sum_i 0.25\,\pi D_i^2 N(D_i) dD_i, \qquad (4)$$

where D_i is the mean diameter of bin size i and $N(D_i)dD_i$ is the number of particles in that bin size and assuming spherical particles. On the basis of Mie theory, $\langle Q_c \rangle$ cannot be larger than 3.2 if all the particles dominating the attenuation were measured [*van de Hulst*, 1957, Figure 32]. A higher value implies that the attenuation is significantly affected by particles outside of the size range measured. In addition, $\langle Q_c \rangle$ should increase with increasing mean particle size for monotonic size distributions, with 2 being its value when only large particles are present (geometric optics limit). The observed average particle attenuation efficiency factors (including particle sizes ranging from 2 to 20 μm, Figure 7) are generally several times higher than the expected values. $\langle Q_c \rangle$ is generally larger in CMO I than in CMO II as both attenuation (Figure 8a) and

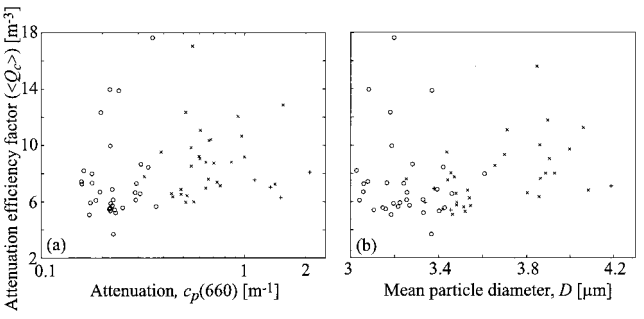

Figure 7. Average particle efficiency factors $\langle Q_c \rangle$ as a function of (a) attenuation and (b) mean particle diameter for CMO I data before the hurricane (crosses), CMO I data after the hurricane (pluses), and CMO II data (open circles). Here $\langle Q_c \rangle$ was computed using (4) with particles of sizes $2 < D < 20\ \mu$.

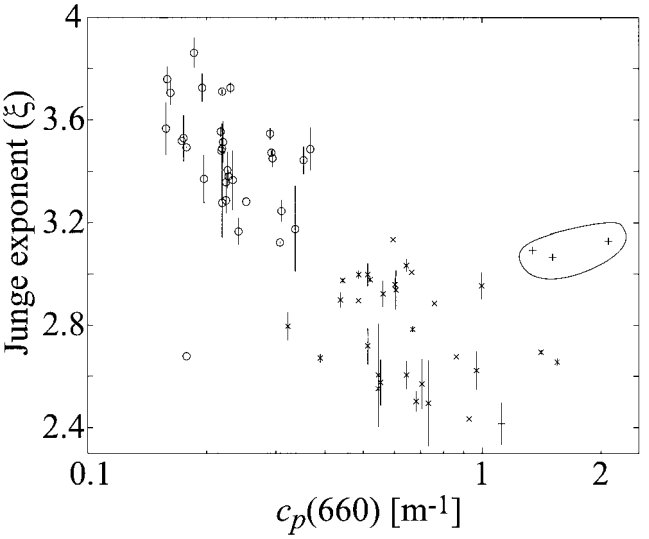

Figure 8. Median (symbols) and two standard deviations (line, when replicates were available) of the PSD exponent ξ of all multisizer samples collected within the BBL as function of attenuation for CMO I data before the hurricane (crosses), CMO I data after the hurricane (pluses), and CMO II data (open circles). The measurements surrounded by a line were collected within the first 25 hours of sampling after the passage of Hurricane Edouard. ξ is based on a nonlinear least squares fit of the measure PSDs to (1) with particles of diameter $2 < D < 20\ \mu$.

mean size (Figure 8b) were higher during CMO I. We also computed directly

$$c_{p,\mathrm{Mie}}(660) = \sum_i 0.25\pi D_i^2 Q_c(660, D_i) N(D_i) dD_i$$

using Mie theory (for Q_c) and compared it to the measured $c_p(660)$. The ratio of computed to measured attenuation ($c_{p,\mathrm{Mie}}(660)/c_p(660)$) was in average 0.27 ± 0.08, consistent with the computed $\langle Q_c \rangle$.

Though we did not have temporally colocated measurements of PSD and spectral particulate attenuation, we used the $\bar{c}_p(660)$ computed from the SlowDROP data and measured with the rosette package to link ξ and γ (Table 1). For the same ranges of attenuation we found that the relationship $\xi = \gamma + 3$ was satisfied within 30% of ξ when ξ is computed for $2 < D < 20\ \mu$ and usually within 10% of ξ when ξ is computed for $3 < D < 20\ \mu$. Figures 3 and 8 imply, through the monotonic relation to $c_p(660)$, that γ and ξ covary monotonously.

4. Discussion

A monotonic inverse relationship between the hyperbolic fit exponent to the particulate attenuation γ and the magnitude of the fit ($\bar{c}_p(660)$) was found in the BBL (Figure 3). This relationship was similar for data from a single site for different seasons and different turbulent intensities (the measured kinetic energy dissipation rates and eddy diffusivities displayed diel changes of 5 orders of magnitudes at the CMO site (M. C. Gregg and J. A. McKinnon, personal communication, 1999). A monotonic $c_p(\lambda_0) - \gamma$ relationship is expected on the basis of idealized approximations of Mie theory. For homogenous, Junge-distributed, nonabsorbing spheres the PSD slope ξ is linearly related to γ. At any given time both $c_p(\lambda_0)$ and ξ change monotonically with distance from the bottom, $c_p(\lambda_0)$ increasing toward the bottom and ξ decreasing toward the bottom (Figure 2), resulting in an inverse monotonic relationship between them in the BBL (Figure 8). The specific $c_p(\lambda_0) - \gamma$ relationship in any given region is expected to depend on the local sediments, as changes in the nature of the particles (density, index of refraction) will cause changes in their optical properties and size distribution.

The two extremes of the $\bar{c}_p(660) - \gamma$ relationship (Figure 3) deserve further discussion. Low values of $\bar{c}_p(660)$ are associated with high values of γ, i.e., relatively more small particles in the water column. These particles are the slowest to sink and characterize the lowest energy state. At the other extreme, the high turbulence energy state, strong resuspension occurs, and there is little change in γ and ξ within the BBL (Figures 3 and 8). Changes are mostly in the concentration of the material in the water, with $\bar{c}_p$ values increasing while only small changes in γ are observed.

Figure 3 introduces a puzzle: why do most of the data follow a single tight relationship? Why are several resuspension events linked through such a tight curve? The evolution of the particulate characteristics in the BBL along the curve after resuspension is most likely due to settling, decreasing $\bar{c}_p(660)$ and increasing the γ. The initial condition for the resuspension need not be on this curve, and many curves could be thought of as possible outcomes. The solution to this puzzle may lie in the aggregation processes (P. Traykowski, personal communication, 1999); aggregation is a fast concentration-dependent process that clears the water rapidly of particles and packages them in faster sinking bigger aggregates [*Kranck*, 1980; *Milligan*, 1995]. As such, it provides a sink for the optical signal as it reduces surface area/volume and removes the particles faster through settling. Such a process may explain the data following the hurricane. Indeed, aggregates were observed to disappear from the BBL in the periods of high turbulence following the hurricane [*Hill et al*., this issue], yet aggregates formed rapidly once shear levels decreased. However, prior to the hurricane and within a day of decreasing shear, aggregates were visible. The strong sensitivity of aggregation to particulate concentration may explain the variability observed between the first and third sampling days following the hurricane (Figure 3).

The range of observed values of γ and ξ (Table 1) is consistent with the linear relationship derived by *Diehl and Haardt* [1980] for idealized particles, $\gamma = \xi - 3$, for $3 < D < 20\ \mu$. Note, however, that the PSD in the entire size range measured by the Coulter device does not have the shape of a Junge-like PSD (i.e., the PSD is not a straight line for all D in Figure 6). Therefore ξ depends on the range of sizes over which we least squares fit (1) (Table 1). In addition, preliminary results based on Mie theory suggest that noticeable deviations from the relationship $\gamma = \xi - 3$ are found for $\xi < 3.3$ and that $\gamma > 0$ for $\xi > 2.5$ (E. Boss and M. S. Twardowski, submitted manuscript, 2000). In all of our data, $\gamma > 0.2$ (Figure 3).

Noticeable changes were observed in $\bar{c}_p(660) - \gamma$ and $c_p(660) - \xi$ relations before and after the hurricane and between the days following the hurricane (Figures 3 and 8). These changes are coincident with changes in the particulate matter to carbon relationship (Blakey et al., submitted manuscript, 2000), indicating that after the hurricane the particle assemblage within the water may have changed. Whether these particles were advected to the Mud Patch or resuspended from deeper within the sediment is unknown, though the sediment at the Mud Patch is known to change as a function of depth [*Twichell et al*., 1987]. Another potential source of different particles may have been the breakup of particle aggregates (see above), possibly causing the increase in chlorophyll in the BBL following Edouard and observed by *Chang et al*. [this issue].

Some of the spread in the $\bar{c}_p(660) - \gamma_{pg}$ relationship may be due to calibration errors. The attenuation slope is very sensitive to CDOM, which could have contaminated the calibration water, affecting the SlowDROP data (comparing Figures 3 and 5a, we find about a 0.13 change in γ_{pg} per 0.01 m^{-1} CDOM absorption at 440). The ac-9 calibration values may have changed when the ac-9 was mounted on the tripod and deployed because of slight changes of the light beam path if the instrument experienced torque, which could affect the correlation between tripod data of different deployments. Indeed, the first deployment data lie on a different $\bar{c}_{pg}(660) - \gamma_{pg}$ curve than the data from the second and fourth deployments (Figure 5b).

In past studies [*Kitchen et al*., 1982; *Spinrad et al*., 1983] the particles measured by a Coulter counter accounted for the bulk of the attenuation measured. For the samples analyzed here, only a small fraction of the attenuation could be explained by the particles sampled, resulting in values of $\langle Q_c \rangle$ much higher than expected (Figure 7). Taken at face value, this means that ~70% of the attenuation is due to particles that were not quantified by the Coulter counter, i.e., particles smaller than 2 μm and larger than 20 μm. In order to test this hypothesis we conducted a numerical study of the potential contribution of the particles that were not sampled. Using a Mie code [*Bohren*

and Huffman, 1983], assuming spherical particles with a real index of refraction of 1.15 (typical of sedimentary particles) and with diameters spanning from 0.02 μ to 250 μm, and PSD with exponents $2.5 < \xi < 4.5$, we found that particles smaller than 2 μm and bigger than 20 μm could contribute between 60 and 80% of the attenuation of the total distribution (depending on the ξ used). These calculations support the hypothesis that the bulk of the attenuation was due to particles that were not measured.

Another possible source of "missing" attenuation may be in the estimation of the volume analyzed by the Coulter counter. In that case the derived ξ will remain unchanged, while the magnitude of the PSD will change. Additionally, PSDs measured in samples collected with a rosette are known to be prone to errors [*McCave*, 1983]; settling within the Niskin bottle [*Gardner*, 1977], aggregation, and disaggregation, all contribute to the differences observed between replicate samples (e.g., Figure 8). A direct comparison between $c_p(660)$ in the BBL and the PSD computed from the water sample is problematic because the vertical gradient in $c_p(660)$ may be very large there. In a few cases, values of attenuation were observed to double in a vertical meter (the vertical dimension of the sampling bottle on the rosette) in the BBL. It is therefore not surprising that the relationship between two colocated in situ optical measurements obtained on the SlowDROP, γ and $\tilde{c}_p(660)$ (Figure 3), is tighter than the relationship between $c_p(660)$ and ξ obtained on the CTD package (Figure 8).

5. Summary and Conclusions

The shapes of the particulate attenuation spectra ($c_p(\lambda)$) were found to be well approximated by a power law with respect to wavelength (Figure 1). While this shape is expected for idealized polydispersed particles, its applicability to measured oceanic assemblages is a new finding. Attenuation was found to be a smooth function of wavelength (Figure 1); it is not strongly influenced by the presence of absorption bands because of a compensating decrease in scattering at those bands [*Kitchen et al*., 1982; *Mueller*, 1973] and is a general property of Mie theory.

A large change in spectral slope is found between the "total" beam attenuation (particulate + CDOM) and the particulate attenuation because of the presence of CDOM in the total beam attenuation. While CDOM makes only a small contribution to the magnitude of the combined attenuation coefficient of particulate and CDOM at any specific visible wavelength, it makes an important contribution to its spectral shape as it typically has an exponentially decreasing attenuation as a function of wavelength. It is thus important to determine accurately CDOM absorption as well as to obtain an accurate calibration for the computation of the shape of the particulate attenuation spectra (for a possible analysis method of separating the two components of total attenuation, see *Barth et al*. [1997]). Alternatively, if the same instrument is used to measure both total and dissolved fractions, the difference, the particulate attenuation, will not be sensitive to calibration.

We have found that c_p and c_{pg} have a simple spectral shape and that the shape, to a large degree, correlates with its magnitude in the BBL. This suggests that given the attenuation at one visible wavelength, it is possible to constrain the attenuation at another wavelength. Similar conclusions can be drawn from past studies of c_{pg} [*Barnard et al*., 1998; *Voss*, 1992].

The results presented here suggest that γ is a sensitive measure of the steepness of the PSD (ξ). For the data presented here a simple linear relationship (3) is found to provide a good prediction to the PSD slope with an average error of <20%. While the relationship of the PSD and particulate attenuation spectrum is known for a specific idealized solution of Mie theory (nonabsorbing, Junge-distributed spherical particles), our results, as well as past studies [*Kitchen et al*., 1982], suggest a wider applicability to oceanic polydispersed particles.

Caution is advised in the applicability of this result to areas were phytoplankton are present in significant numbers in that phytoplankton are strong absorbers and have the potential for skewing the particulate population toward highly non-Jungian distributions. Nonetheless, our data suggest that for detrital particles and for a certain range of attenuation magnitudes, visible attenuation may provide enough information to perform inversions to calculate the parameters of the PSD, in contrast to the larger bandwidth required by other known inversion methods [*Shifrin*, 1988].

Notation

a_p	particulate absorption, m^{-1}.
a_g	dissolved absorption, m^{-1}.
a_{pg}	particulate plus dissolved absorption, $a_{pg} = a_{p+}a_g$, m^{-1}.
b_p	particulate scattering, m^{-1}.
c_p	particulate attenuation, $c_{p=}\ a_{p+}\ b_p$, m^{-1}.
$\tilde{c}_p(660)$	magnitude of nonlinear fit (3) to the particulate attenuation at 660 nm measured with the SlowDROP, m^{-1}.
$c_{p,\mathrm{Mie}}$	attenuation computed on the basis of observed size distribution and Mie theory.
c_{pg}	particulate plus dissolved attenuation, computed by $c_{pg} = c_{p+}a_g$, m^{-1}.
$\tilde{c}_{pg}(660)$	magnitude of nonlinear fit to the particulate plus dissolved attenuation at 660 nm measured with the ac-9, m^{-1}.
D	diameter, m.
D_0	reference diameter, m.
N	number of particles per unit volume per length interval, number per m^4.
N_0	$N(D_0)$, number per m^4.
Q_c	attenuation efficiency factor, m^{-3}.
γ	slope of the hyperbolic fit to c_p (3), dimensionless.
γ_{pg}	slope of the hyperbolic fit to c_{pg} (3), dimensionless.
λ	wavelength, nm.
λ_0	reference wavelength, nm.
σ_t	density (ρ) − 1000, kg m^{-3}.
ξ	slope of the hyperbolic fit to the PSD, dimensionless.

Acknowledgments. This research has been supported as part of the Coastal Mixing and Optics program of the Office of Naval Research. We thank Joshua Blakey and Jan Gundersen for running the Coulter size samples. We thank Peter Traykowsky, Paul Hill, and Heidi Sosik for valuable discussions.

References

Barnard, A. H., W. S. Pegau, and J. R. V. Zaneveld, Global relationships of the inherent optical properties of the oceans, *J. Geophys. Res*., *103*, 24,955–24,968, 1998.

Barth, H., K. Grisard, K. Holtsch, R. Reuter, and U. Stute, Polychromatic transmissometer for in situ measurements of suspended particles and gelbstoff in water, *Appl. Opt*., *36*, 7919–7928, 1997.

Bohren, C. F., and D. R. Huffman, *Absorption and Scattering of Light by Small Particles*, 530 pp., John Wiley, New York, 1983.

Boss, E., W. S. Pegau, J. R. V. Zaneveld, and A. H. Barnard, Spatial and temporal variability of absorption by dissolved material at a continental shelf, *J. Geophys. Res*., this issue.

Chang, G. C., and T. D. Dickey, Optical and physical variability on timescales from minutes to the seasonal cycle on the New England continental shelf: July 1996 to June 1997, *J. Geophys. Res*., this issue.

Chang, G. C., T. D. Dickey, and A. J. Williams III, Sediment resuspension over a continental shelf during Hurricanes Edouard and Hortense, *J. Geophys. Res*., this issue.

Culver, M. E., and M.-J. Perry, The response of photosynthetic absorption coefficients to irradiance in culture and in tidally mixed estuarine waters, *Limnol. Oceanogr*., *44*, 24–36, 1999.

Dickey, T. D., G. C. Chang, Y. C. Argawal, A. J. Williams III, and P. S. Hill, Sediment resuspension in the wakes of Hurricanes Edouard and Hortense, *Geophys. Res. Lett*., *25*, 3533–3536, 1998.

Diehl, P., and H. Haardt, Measurement of the spectral attenuation to support biological research in a "plankton tube" experiment, *Oceanol. Acta*, *3,* 89–96, 1980.

Gardner, W. D., Incomplete extraction of rapidly settling particles from water samples, *Limnol. Oceanogr*., *22*, 764–768, 1977.

Gardner, W. D., I. D. Walsh, and M. J. Richardson, Biophysical forcing and particle production and distribution during a spring bloom in the North Atlantic, *Deep Sea Res*., *Part II*, *40*, 171–195, 1993.

Gardner, W. D., et al., Optics, particles, stratification, and storms on the New England continental shelf, *J. Geophys. Res.*, this issue.

Hill, P. S., G. Voulgaris, and J. H. Trowbridge, Controls on floc size in a continental shelf bottom boundary layer, *J. Geophys. Res*., this issue.

Kitchen, J. C., J. R. V. Zaneveld, and H. Pak, Effect of particle size distribution and chlorophyll content on beam attenuation spectra, *Appl. Opt*., *21*, 3913–3918, 1982.

Kranck, K., Experiments on the significance of flocculation in the settling of fine-grained sediment in still water, *Can. J. Earth Sci*., *17*, 1517–1526, 1980.

McCave, I. N., Particulate size spectra, behavior, and origin of nephloid layers over the Nova Scotia continental rise, *J. Geophys. Res*., *88*, 7647–7666, 1983.

Middleton, G. V., and J. B. Southard, *Mechanics of Sediment Movement*, Soc. for Sediment. Geol., Providence, R. I., 1984.

Miller, M. C., I. N. McCave, and P. D. Komar, Threshold of sediment motion under unidirectional currents, *Sedimentology*, *24*, 507–527, 1977.

Milligan, T. G., An examination of the settling behaviour of a flocculated suspension, *Neth. J. Sea Res*., *33*, 163–171, 1995.

Moore, C., E. J. Bruce, W. S. Pegau, and A. D. Weidemann, Wet Labs ac-9: Field calibration protocol, deployment techniques, data processing and design improvements, *Proc. SPIE Int. Soc. Opt. Eng*., *13*, 725–730, 1996.

Morel, A., Diffusion de la lumiere par les eaux de mer: Resultats experimentaux et approche theorique, in *AGARD Lect. Ser*., *61*, 3.1.1–3.1.76, 1973.

Mueller, J. L., The influence of phytoplankton on ocean color spectra, Ph.D. thesis, Oregon State Univ., Corvallis, 1973.

Pak, H., J. R. V. Zaneveld, and J. Kitchen, Intermediate nepheloid layers observed off Oregon and Washington, *J. Geophys. Res*., *85*, 6697–6708, 1980.

Rouse, H., Modern conceptions of the mechanics of turbulence, *Trans. Am. Soc. Civ. Eng*., *102*, 436–505, 1937.

Shifrin, K. S., *Physical Optics of Ocean Water*, 285 pp., Am. Inst. of Phys., New York, 1988.

Spinrad, R. W., J. R. V. Zaneveld, and J. C. Kitchen, A study of the optical characteristics of the suspended particles in the benthic nephloid layer of the Scotian shelf, *J. Geophys. Res*., *88*, 7641–7645, 1983.

Stramski, D., and C. D. Mobley, Effects of microbial particles on oceanic optics: A database of single-particle optical properties, *Limnol. Oceanogr*., *42*, 538–549, 1997.

Twardowski, M. S., J. M. Sullivan, P. L. Donaghay, and J. R. V. Zaneveld, Microscale quantification of the absorption by dissolved and particulate material in coastal waters with an ac-9, *J. Atmos. Oceanic Technol.*, *16*, 691–707, 1999.

Twichell, D. C., B. Butman, and R. S. Lewis, Shallow structure, surficial geology, and the processes currently shaping the bank, in *Georges Bank*, edited by R. H. Backus, pp. 31–37, MIT Press, Cambridge, Mass., 1987.

van de Hulst, H. C., *Light Scattering by Small Particles*, Dover, Mineola, N. Y., 1957.

Volz, F., Die Optik und Meteorologie der atmosphärishen Trubung, *Ber. Dtsch. Wetterdienstes*, *13*, 1–47, 1954.

Voss, K. J., A spectral model of the beam attenuation coefficient in the ocean and coastal areas, *Limnol. Oceanogr*., *37*, 501–509, 1992.

Zaneveld, J. R. V., J. C. Kitchen, and C. C. Moore, Scattering error correction of reflecting tube absorption meters, *Proc. SPIE Int. Soc. Opt. Eng*., *12*, 44–55, 1994.

H. Barnard, E. Boss, W. S. Pegau, M. S. Twardowski, and J. R. V. Zaneveld, College of Ocean and Atmospheric Sciences, Oregon State University, 104 Ocean Administration Bldg., Corvallis, OR 97331. (boss@oce.orst.edu)

G. C. Chang, Florida Environmental Research Institute, 4807 Bayshore Boulevard, Suite 101, Tampa, FL 33611.

T. D. Dickey, Ocean Physics Laboratory, University of California, Santa Barbara, 6487 Calle Real Unit A, Goleta, CA 93117.

W. D. Gardner, Department of Oceanography, Texas A&M University, College Station, TX 77843–3146.

(Received June 25, 1999; revised March 6, 2000;
accepted March 9, 2000.)